Enhancements to the open access spectral band adjustment factor online calculation tool for visible channels

Benjamin Scarino*[a], David R. Doelling[b], Arun Gopalan[a], Thad Chee[a], Rajendra Bhatt[a], Conor Haney[a]

[a]SSAI, One Enterprise Pkwy Ste 200, Hampton, VA 23666 USA

[b]NASA Langley Research Center, 21 Langley Blvd MS 420, Hampton, VA 23681-2199 USA

ABSTRACT

With close to 40 years of satellite observations, from which, cloud, land-use, and aerosol parameters can be measured, inter-consistent calibrations are needed to normalize retrievals across satellite records. Various visible-sensor inter-calibration techniques have been developed that utilize radiometrically stable Earth targets, e.g., deep convective clouds and desert/polar ice pseudo-invariant calibration sites. Other equally effective, direct techniques for inter-calibration between satellite imagers are simultaneous nadir overpass comparisons and ray-matched radiance pairs. Combining independent calibration results from such varied techniques yields robust calibration coefficients, and is a form of self-validation. One potential source of significant error when cross-calibrating satellite sensors, however, are the often small but substantial spectral discrepancies between comparable bands, which must be accounted for. As such, visible calibration methods rely on a Spectral Band Adjustment Factor (SBAF) to account for the spectral-response-function-induced radiance differences between analogous imagers. The SBAF is unique to each calibration method as it is a function of the Earth-reflected spectra. In recent years, NASA Langley pioneered the use of SCIAMACHY-, GOME-2-, and Hyperion-retrieved Earth spectra to compute SBAFs. By carefully selecting hyperspectral footprints that best represent the conditions inherent to an inter-calibration technique, the uncertainty in the SBAF is greatly reduced. NASA Langley initially provided the Global Space-based Inter-calibration System processing and research centers with online SBAF tools, with which users select conditions to best match their calibration criteria. This article highlights expanded SBAF tool capabilities for visible wavelengths, with emphasis on the use of the spectral range filtering for the purpose of separating scene conditions for the channel that the SBAF is needed based on the reflectance values of other bands. In other words, spectral filtering will enable better scene-type selection for bands where scene determination is difficult without information from other channels, which should prove valuable to users in the calibration community.

1. INTRODUCTION

The online, open-access web tool for user-guided calculation of spectral band adjustment factors (SBAFs) satisfies a critical need of the Global Space-based Inter-calibration System (GSICS) organization, as well as the broader calibration community (*https://satcorps.larc.nasa.gov/SBAF*)[1,2]. A pre-processed, database-driven online tool allows users the flexibility to design SBAFs that are unique to their sensor and calibration targets as needed. Subtle computation variations are easy to test without requiring a time-consuming reprocess. The calibration community has an opportunity to utilize a consistent and well-documented SBAF algorithm, rather than consuming valuable resources in employing their own techniques, or to use the tool as a validation check on their methods. The one-stop, on-the-fly web tool gives users open access to a critical calibration asset that can easily be referenced and tested for a multitude of calibration efforts.

The concept of the SBAF, which is to account for analogous sensor spectral band differences, is well established within the actively monitored and invariant surface site calibration communities[3]. Radiative transfer models (RTM) have been the traditional means of achieving the adjustment – models which rely on well-characterized surface reflectance and atmospheric measurements to predict the at-sensor spectra during the satellite overpass[4,5,6,7]. Although generally reliable, the ground reflectance measurement and the inherent accuracy of the RTM are the greatest sources of uncertainty for this method – estimated at 1.6% and 2.0%, respectively[8]. More significant is the question of whether the model adequately represents one's specific calibration scene in terms of spectral signature. Furthermore, active

Keywords: SBAF, SCIAMACHY, Hyperspectral, Inter-calibration, Visible

*benjamin.r.scarino@nasa.gov; phone 1 757 951-1622; fax 1 757 951-1902

monitoring of a site can be an expensive operation. A more economical and effective way of deriving scene-specific SBAFs is achieved using satellite hyperspectral sensor data. Although having adequate simultaneous data from a hyperspectral instrument during a satellite inter-calibration event is often not feasible, it was found that using hyperspectral radiances with the same angular and scene conditions as that during the event provided similar SBAFs to those that were acquired simultaneously[7]. This is a reasonable assumption considering that only relative changes, i.e., non-uniform or non-absolute, within the hyperspectral signature would affect integrated spectra comparisons, unless sensor degradation is significant. The development of predetermined SBAFs based on hyperspectral radiance observations, specifically from the Envisat Scanning Imaging Absorption spectroMeter for Atmospheric CHartographY (SCIAMACHY), was pioneered by the Clouds and the Earth's Radiant Energy System (CERES) and Climate Absolute Radiance and Refractivity Observatory (CLARREO) calibration groups[1,9,10]. Careful selection of footprints that closely match scene conditions specific to the inter-calibration event is the key to success when deriving SBAFs from hyperspectral observations.

Given their overlapping records and analogous bands, the Aqua Moderate Resolution Imaging Spectroradiometer (MODIS) and National Polar-orbiting Partnership Visible Infrared Imaging Radiometer Suite (NPP-VIIRS) have been endorsed by the GSICS community as visible calibration references with which to normalize all contemporary sensors[11,12]. The goal is to then join this series with the future CLARREO SI traceable calibration[13]. It has been common practice to rely on all-sky tropical ocean (ATO) scenes for deriving inter-consistent calibration coefficients between target geostationary satellite sensors and reference instruments like MODIS and VIIRS[14]. We have recently found, however, that ATO scenes may be unsuitable for calibrating certain visible channels due to difficulty in spectrally characterizing the mixed cloud/ocean views in the collocated instrument footprints. An appropriate SBAF is therefore difficult to derive when there is low sensitivity to scene-specific energy thresholds at the wavelength of interest. To solve this problem, one can filter the target channel for a certain scene type based on better-defined, scene-specific energy thresholds of a separate reference spectral range. In this article, consistency of calibration coefficients achieved via careful SBAF selection based on spectral filtering for varied scene types will serve as a simple application demonstration of enhanced SBAF tool filtering features.

2. METHODOLOGY

2.1 Spectral Band Adjustment Factor (SBAF)

An accurate, well-characterized SBAF between analogous bands will account for the Earth-reflected spectral differences between those bands. The Earth-reflected spectra are a function of the solar incoming spectral irradiance (Fig. 1a), and the reflective/absorptive properties of the surface and atmosphere (Fig. 1b). From Fig. 1b, this pattern implies that the computed SBAF between Geostationary Operational Environmental Satellite (GOES) -12 Channel 1 and MODIS Band 1 (both centered ~0.65 μm) would differ depending on whether the adjustment is determined from deep convective clouds (DCC), vegetation, or ocean scenes. The SBAF relies on parameters computed from true hyperspectral instrument radiances (L), scaled radiances (radiance divided by the solar radiance), or brightness temperatures (BT; for infrared-channel SBAFs) convolved with the target/reference instrument SRFs. The parameters should therefore be spectrally comparable to the true target/reference instrument, and hence are deemed *pseudo* instrument parameters. That is, the spectra from the given hyperspectral instrument footprint must be carefully convolved with the SRFs of both the reference and target imager channels in order to compute imager-equivalent, or pseudo, radiance, scaled radiance (reflectance), or BT values.

The complete SBAF methodology as designed for SCIAMACHY is summarized by Scarino et al. (2016). Equation 1 shows the derivation of a target-sensor pseudo radiance ($L_{p,tar}$):

$$L_{p,tar} = \frac{\sum_{n}^{nbins} L_{s,n} \times RSR_{tar,n} \times (\lambda_n - \lambda_{n-1})}{\sum_{n}^{nbins} RSR_{tar,n} \times (\lambda_n - \lambda_{n-1})}, \qquad (1)$$

where $L_{s,n}$ is the hyperspectral instrument at-sensor radiance for hyperspectral wavelength bin n, $nbins$ is the total number of wavelength bins that defined the hyperspectral instrument spectral resolution, and $RSR_{tar,n}$ is the target relative spectral response (same as SRF) at that same wavelength (λ). The reference pseudo radiance $L_{p,ref}$ is calculated similarly with Eq. 1, except using the reference SRF. The regression analysis of the pseudo radiance target and reference pairs, with $L_{p,tar}$ as the ordinate and $L_{p,ref}$ as the abscissa, will yield an SBAF for the target-reference pair over the selected Earth spectra. In the tool (see section 2.3), the user can select the regression type (degree of polynomial) that most effectively captures the variability of the pseudo radiance pairs, with care not to over/under characterize the relationship. The SBAF

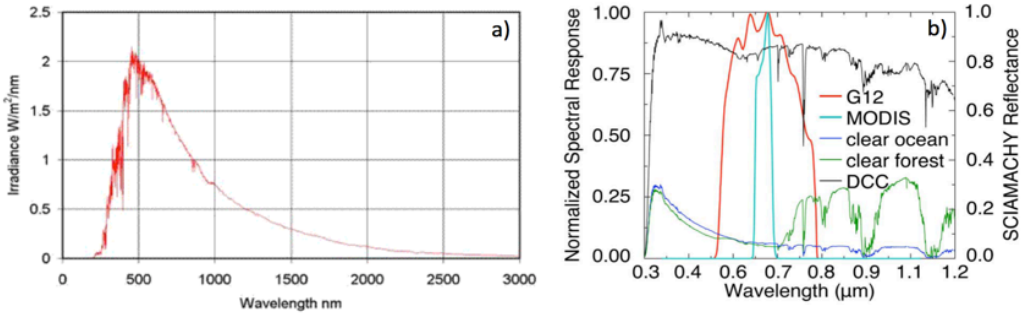

Figure 1. a) The 1985 Wehrli Standard Extraterrestrial Solar Irradiance Spectrum. b) Examples of SCIAMACHY reflectance spectra over deep convective clouds, clear-sky ocean, and vegetation overlaid with GOES-12 channel 1 (G12) and MODIS band 1 SRFs.

is applied to the true, i.e., not pseudo, reference-sensor radiance (L_{ref}) in order to arrive at a predicted target-sensor radiance ($L_{tar,predict}$) as shown in Eq. 2:

$$L_{tar,predict} = SBAF \times L_{ref}. \qquad (2)$$

For Eq. 2, the SBAF term represents a simple ratio of average $L_{p,tar}$ to average $L_{p,ref}$. Usually, higher degree polynomial regressions are needed to properly account for the spectral band differences, thereby allowing the SBAF to realistically vary as a function of radiance.

2.2 Spectra Plotting and Filtering Tool

The SCIAMACHY Version-1 spectra plotting and SBAF (see section 2.3) web tools were developed at NASA Langley to satisfy a need for frequent specialized spectra visualization and instrument spectral difference corrections, built with consideration for a continually growing library of imagers and channels. The publicly available tools can be found at *https://satcorps.larc.nasa.gov* under the *Langley Satellite Calibration* link, along with other useful calibration resources and assets. Comparable visible-wavelength plotting tools are also available for the Global Ozone Monitoring Experiment–2 (GOME-2) and Hyperion hyperspectral instruments, while the Infrared Atmospheric Sounding Interferometer (IASI) and Atmospheric Infrared Sounder (AIRS) based tools cover SBAFs for infrared channels.

The spectra plotting tool is useful for visualizing the available SCIAMACHY mean hyperspectral radiance or scaled radiance (i.e., reflectance) Earth-reflected spectra signature. Options for Earth-reflected spectra include, but are not limited to, all-sky and clear-sky tropical ocean, all-sky and clear-sky land based on International Geosphere-Biosphere Programme (IGBP) land use designations and pseudo-invariant calibration sites (PICS), and various cloud types including DCC. The current tool interface is shown in Fig. 2, with which users have options to control specific aspects of the plotted spectra, such as sun angle and satellite viewing angle. A particularly useful feature is the capability to control what footprint spectra are allowed in the mean signature by filtering either radiance or reflectance values within a specified wavelength range. That is, any individual SCIAMACHY spectra with a measured value outside of an indicated minimum/maximum radiance or minimum/maximum reflectance within the range minimum/maximum μm (i.e., μm signifying wavelength) will be excluded from the spectral averaging. Users can employ up to two of these spectral filters, which can be used to separate scene conditions in one band range based on the radiance/reflectance values within a completely separate range of wavelengths (see Section 2.4). By using spectral filter wavelength ranges that closely resemble actual instrument channels, the filtering criteria can then be used on those same sensor channels in order to select the desired coincident, angle-matched inter-calibration pairs.

2.3 SBAF Tool

The current SCIAMACHY SBAF web tool interface is shown in Fig. 3, with which users can tailor an SBAF to best suit the need of their calibration event by selecting the Earth-reflected spectra along with a reference (regression x-axis) and target (regression y-axis) instrument/channel SRF. The plotting unit type (pseudo radiance or pseudo scaled radiance) and regression form (e.g., forced linear through the origin to 3rd-order non-linear) must also be specified in order to produce a basic SBAF figure. More advanced subsetting options, including angle limits, precipitable water amount, geolocation and date range, uncertainty thresholds, and plotting controls (data plotting bounds and axis limits)

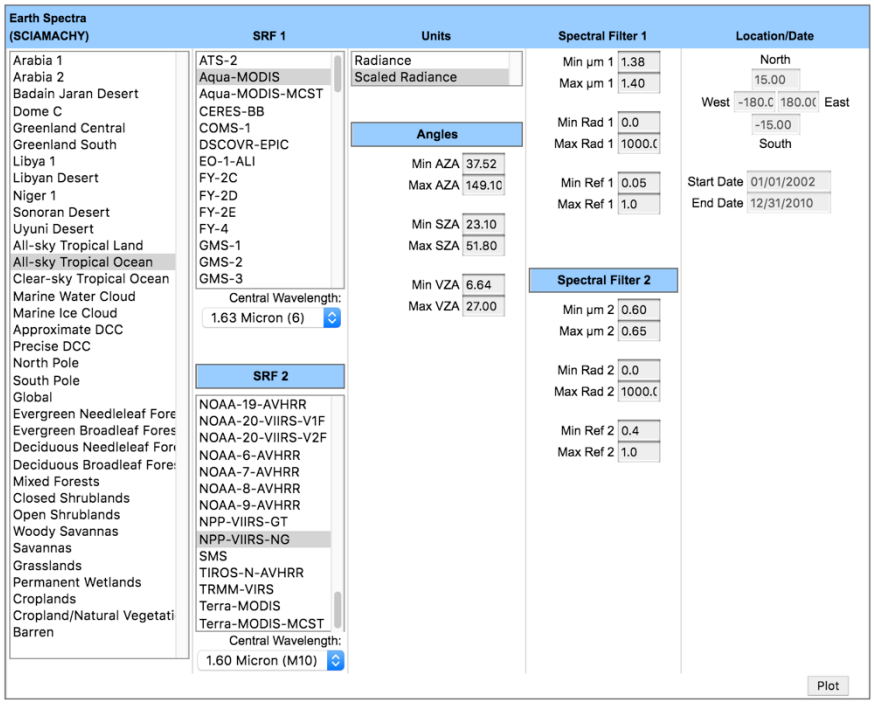

Figure 2. The Version 1.3 SCIAMACHY spectra plotting tool web interface.

can be further refined when such conditions will produce a better SBAF, e.g., when specifically designed for the users' inter-calibration events. Furthermore, the same spectral filtering capabilities introduced to the spectral plotting tool are enabled in the SBAF tool, which allow users to generate an SBAF for all channel pairings using any single or double spectral filtering scheme desired, especially for channel pairs that are distinct from the filtering wavelengths. The complementary design of these tools should prove beneficial to users, starting with the visualization of the spectral filter in the spectra plotting tool, and then subsequent application using the SBAF tool.

2.4 Simple Application Demonstration - MODIS and VIIRS Comparison

In recent years, various Aqua-MODIS and NPP-VIIRS inter-calibration methods have been utilized to radiometrically scale the MODIS and VIIRS analogous bands. Some methods rely on homogenous scene conditions that are known to be stable over time, such as deserts, polar ice targets, and DCC. Other methods rely on simultaneous nadir overpass (SNO) comparisons between the two sensors. The scene type during these SNO events can vary greatly, depending on the surface and cloud conditions at the overpass locations. Different SNO events have different top-of-atmosphere reflected solar spectra, and each requires their own unique SBAF. Put simply, the disparity of spectral signatures between analogous channels can vary significantly depending on wavelength and target.

NASA-Langley has used ATO MODIS and VIIRS coincident, angle-matched radiance pairs to radiometrically normalize the two sensors. All-sky tropical ocean conditions are comprised of varied scene types, such as marine water clouds (MWC), marine ice clouds (MIC), and clear-sky tropical ocean (CTO) components, each of which have distinct spectral features. It was observed, however, that for the 0.65-µm bands, the three scene types can be stratified by the radiance. That is, very low radiance values are observed over CTO, MWC scenes cover the mid-range of radiances, and MIC consists of the highest radiance values. There still remains, nevertheless, considerable radiance overlap between the three environments. With a 2nd-order regression SBAF applied for the MODIS and VIIRS radiance pairs, spectral correction is a function of radiance magnitude, and, as such, when comparing the radiometric scaling between ATO SNOs, DCC, and deserts, the scaling is found to be similar. The 2nd-order SBAF assumption may not hold for other bands, however, and perhaps an improved 0.65-µm SBAF can be formulated.

The goal of this study is to improve upon the practice of using a single SBAF for all of the scene conditions observed within the ATO pairings. This objective is accomplished by computing SBAFs specifically for MWC, MIC, and CTO environments, and employing those SBAFs under comparable inter-calibration conditions. As such, the

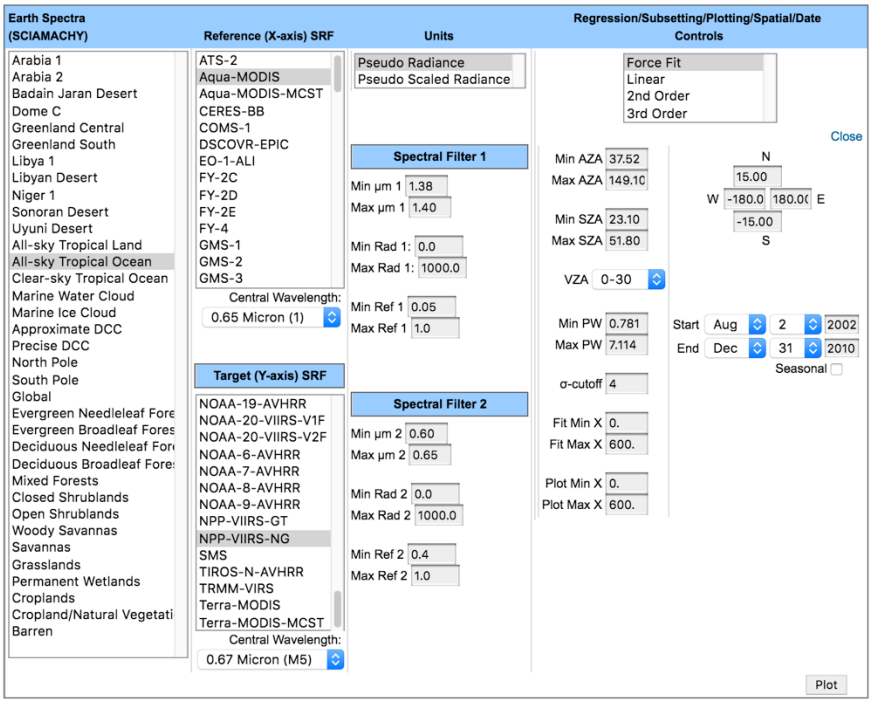

Figure 3. The Version 1.5 SCIAMACHY SBAF tool web interface.

greatest challenge is the reliable selection of MODIS/VIIRS radiance pairs for the specific scene types, for which to apply the appropriate SBAF. If the scene types cannot be reliably identified, then the attempted SBAF may be less accurate in application than that of using the overall ATO SBAF. As such, the SBAF improvement is thus limited by the number of scene types that can be reliably classified, as well as by the magnitude of the scene spectral variation. The target scenes are classified via spectral filtering of the sensor bands that offer the greatest radiance or reflectance stratification, which are not necessarily the same as those bands being scaled. The scene-specific SBAF values are highly dependent on wavelength, and as such, the required adjustment can vary significantly from channel to channel.

Simultaneous nadir overpass comparisons between MODIS and VIIRS are used to assess the effectiveness of the spectral filters used to distinguish scene conditions for ray-matched observations, and their respective SBAFs, in the 0.65-µm and 1.6-µm bands. The SNOs are acquired over ATO from -30º to +30º latitude for orbit intersections within 15 minutes, and for viewing and solar zenith angle differences less than 3º. Relative azimuth angle difference allowance ranges from 3º for the darkest 1/3rd of matches, 5º for the middle 1/3rd, to 10º for the brightest 1/3rd. Stratifying the angular matching allowance by radiance thresholds accounts for the greater frequency of clear-sky pairs compared with those from bright clouds (i.e., reducing the low-end sampling weight). Conveniently, the clear-sky scenes are rather anisotropic compared to bright clouds and thus already benefit from strict angle matching, whereas angle matching over bright clouds can be less constrained. Pixel radiance values from each sensor are averaged inside a 50-km diameter within the angular constraints before comparison, and then compiled annually and regressed to determine the scaling relationship. A regression of the annually averaged scaling relationship reveals the mean gain and any calibration drift. The goal is to use the spectral filtering capabilities of the SCIAMACHY spectra plotting and SBAF tools to separate the MODIS and VIIRS ATO SNOs into their MWC, MIC, and CTO components, each requiring a unique SBAF based on the same spectral filtering criteria. The MODIS and VIIRS relative radiometric scaling, or gain, is determined from the MWC, MIC, and CTO scenes with their specific SBAF applied. The gains compared to the ATO SNO scaling, as well as the consistency among MWC, MIC and CTO gains, reveals the effectiveness of the spectral filtering method.

In order to assess how well spectrally filtered SBAFs can aid in determining a more precise MODIS and VIIRS SNO calibration relationship, we first attempt to replicate the signature of particular Earth-reflected spectra using a non-specific scene type. The general, or non-specific scene type, for the MODIS and VIIRS SNO matches is ATO, of which any field of view will contain some combination of MWC, MIC, and CTO scenes. The ATO spectral signature, which is already included in the SCIAMACHY spectra plotting tool, is shown in Fig. 4a, with corresponding pseudo radiance pair SBAF regressions shown for the MODIS and VIIRS 0.65-µm (Fig. 4b) and 1.6-µm (Fig. 4c) channels. The relatively

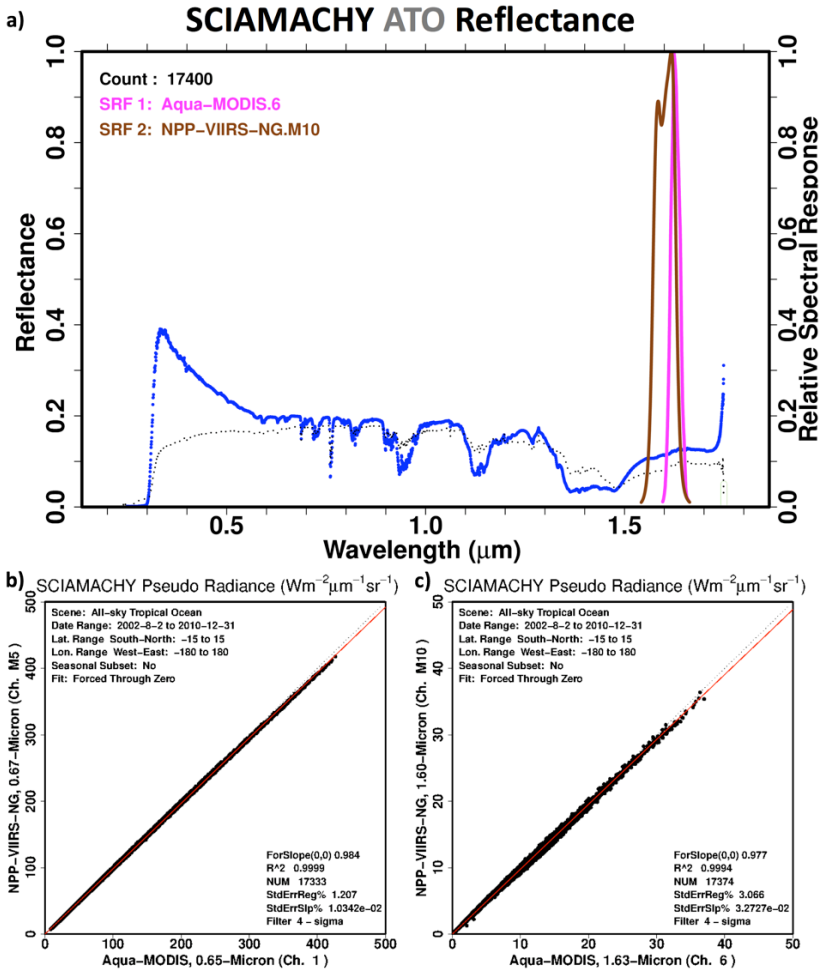

Figure 4. a) SCIAMACHY ATO Earth-reflected spectra signature with overlaid MODIS and VIIRS 1.6-μm channels SRFs. The blue dots indicate the mean reflectance, and the grey dots indicate the standard deviation. b) A 0.65-μm channel pseudo radiance pair SBAF regression for the ATO scene. c) Same as b) except instead for the 1.6-μm channel.

large magnitude of the grey dotted line in Fig. 4a, which indicates the ATO reflectance standard deviation, suggests a significant mixture of high and low reflectance values sourced from the composite of MWC, MIC, and CTO scenes.

The SCIAMACHY spectra plotting tool has built-in Earth-reflected spectra signatures for MWC, MIC, and CTO, which are shown in Figs. 5a, 5c, and 5e, respectively. These pre-built scenes were made specifically for the tool using cloud temperature and optical depth thresholds determined from Terra CERES 20-km Level-2 Single Scanner Footprint Edition 2 cloud retrievals[1]. It must be noted that the SCIAMACHY footprints are large (30 km x 240 km), therefore making identification of homogenous footprints difficult, especially for CTO where residual cloud contamination is common. Also, the Terra satellite, which has a 10:30 AM local equator crossing time (LECT), is not in the same orbit as Envisat (10:00 AM LECT). The slight orbital time difference may introduce a mismatch between the MODIS cloud properties and SCIAMACHY spectral radiance. Perfect agreement between spectral filtering and scene identification based on MODIS cloud properties is not expected.

Figures 5b, 5d, and 5f, respectively, are attempted replicas of the pre-built MWC, MIC, and CTO scenes, constructed using the general ATO signature along with a double spectral filtering scheme. That is, two spectral filters based on minimum/maximum μm (see Fig. 2) ranges of 0.60-0.65-μm (green tick-marks in Fig. 5), and 1.38-1.40-μm (red tick-marks in Fig. 5), with varying minimum/maximum reflectance thresholds allow for approximate replication of the MWC, MIC, and CTO pre-built SCIAMACHY signatures. In a qualitative sense, the filters are effective in producing MWC (5a vs. 5b), MIC (5c vs. 5d), or CTO (5e vs. 5f) replicas from the ATO scene.

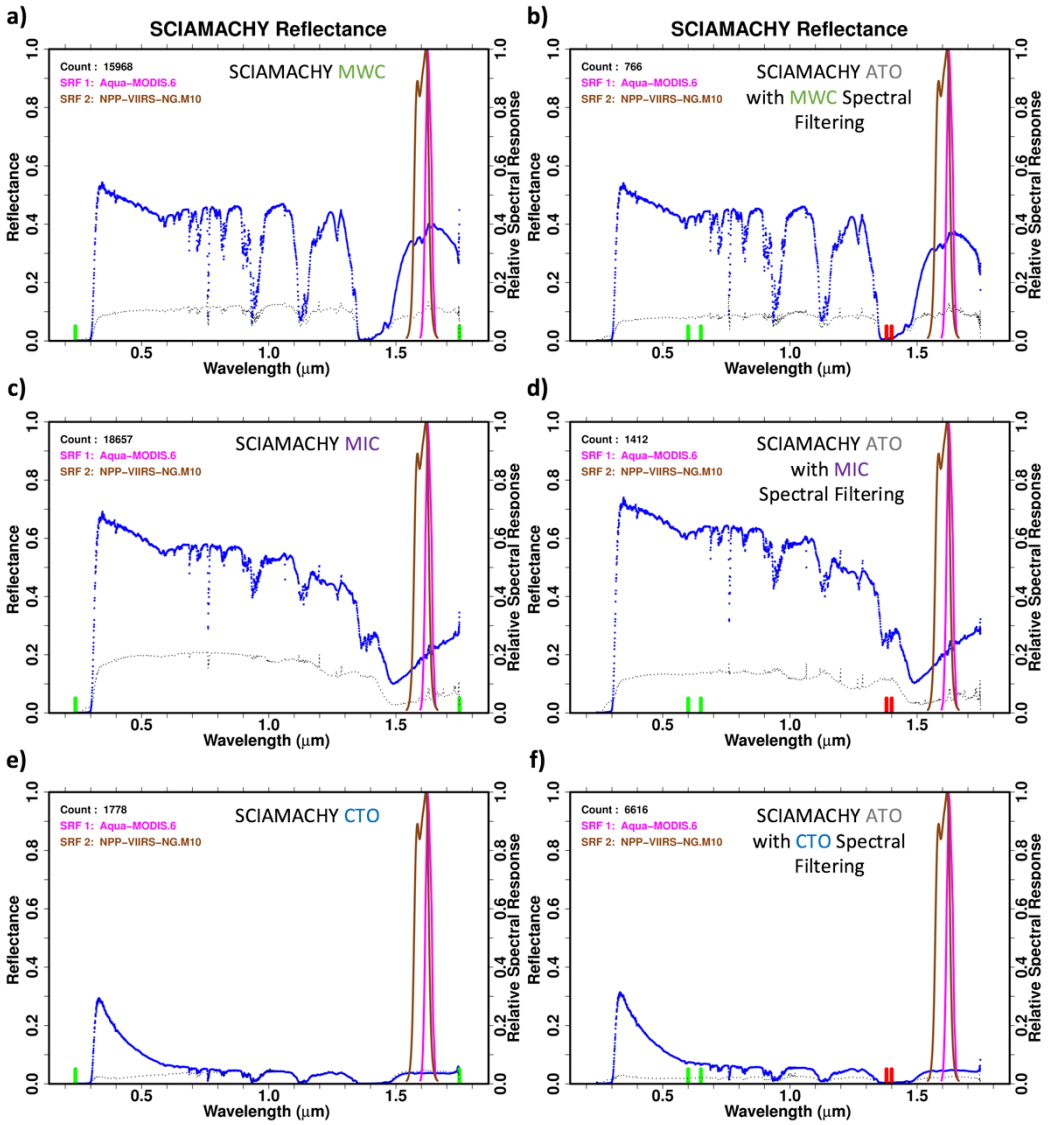

Figure 5. a), c) and e) Pre-determined SCIAMACHY Earth-reflected MWC, MIC, and CTO spectral signatures. b), d), and f) SCIAMACHY Earth-reflected ATO spectra signatures spectrally filtered to approximate the MWC, MIC, and CTO signatures. The red and green x-axis tick-marks indicate the wavelength range over which each of the two spectral filters operate. If no spectral filter is specified, then green tick-marks appear at the extreme ends of SCIAMACHY spectral range. The blue dots represent the averaged reflectance spectra with the gray dots indicating the standard deviation. The count is the number of SCIAMACHY footprints used to compute the average. The brown and pink lines represent the relative spectral response functions of the selected sensor bands, and are labeled in the upper left corner of each plot.

The specific thresholds for MWC, MIC, and CTO spectral filtering are shown in Table 1. These thresholds are determined by qualitative comparison of the paired spectral signatures combined with a quantitative assessment of the minimal difference in the computed SBAF from each scene, considering both the 0.65-μm and 1.6-μm channels (Figs. 6 and 7, respectively). That is, the SBAFs from the pre-determined SCIAMACHY MWC and the MWC-equivalent ATO case are the same for both channels (6a vs. 6b and 7a vs. 7b), and for MIC case the SBAF difference is only 0.1% for both channels (6c vs. 6d and 7c vs. 7d). For the CTO case, however, the minimum SBAF difference when considering both the 0.65-μm and 1.6-μm channels is 0.7% and 0.9%, respectively (6e vs. 6f and 7e vs. 7f).

Table 1. The wavelength ranges (μm) and minimum/maximum reflectance values used for spectral filters 1 and 2 to come up with the MWC-, MIC-, and CTO-equivalent scenes using ATO Earth-reflected spectra, as seen in Figs. 5b, 5d, and 5f, respectively.

	Spectral Filter 1			Spectral Filter 2		
	Range (μm)	Min Ref.	Max Ref.	Range (μm)	Min Ref.	Max Ref.
MWC	1.38-1.40	0.00	0.05	0.60-0.65	0.30	1.00
MIC	1.38-1.40	0.05	1.00	0.60-0.65	0.40	1.00
CTO	1.38-1.40	0.00	0.05	0.60-0.65	0.00	0.11

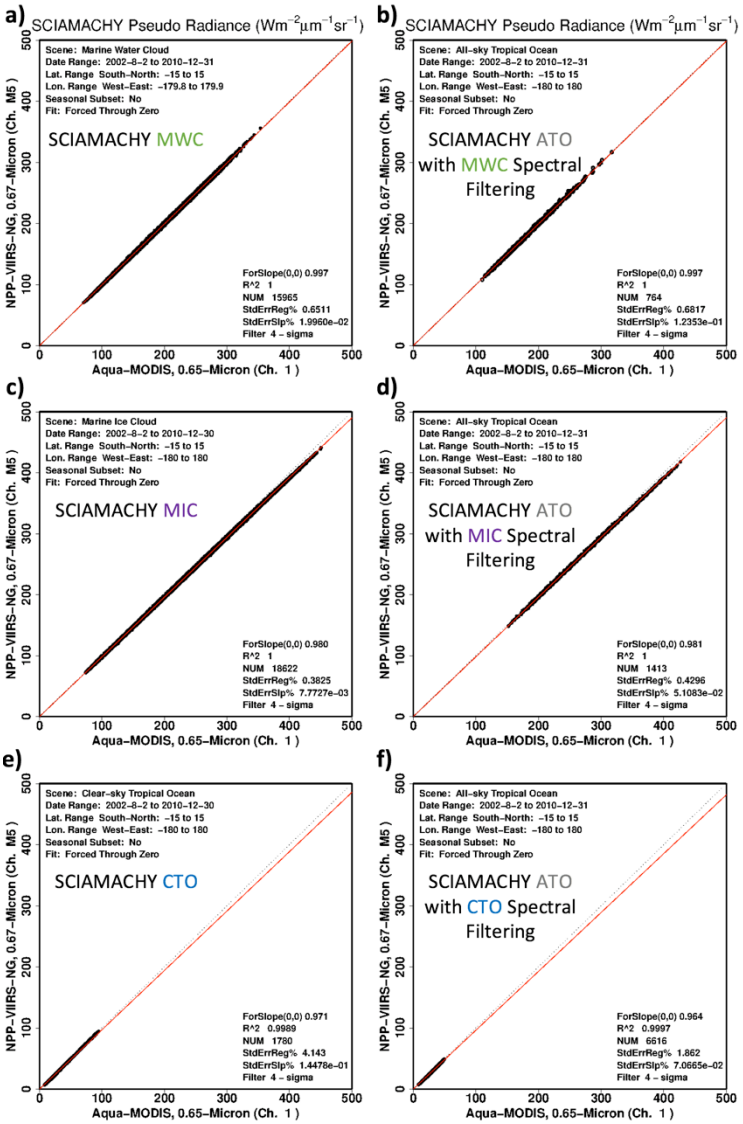

Figure 6. a), c) and e) Pre-determined SCIAMACHY Earth-reflected MWC, MIC, and CTO signature pseudo radiance regressions (i.e., SBAFs) for Aqua-MODIS band 1 and NPP-VIIRS band M5. b), d), and f) SCIAMACHY Earth-reflected ATO SBAFs for the same bands spectrally filtered to approximate the pre-determined MWC, MIC, and CTO signature SBAFs. The red line illustrates the SBAF regression, whereas the black points represent the SCIAMACHY footprint pseudo radiance pairs.

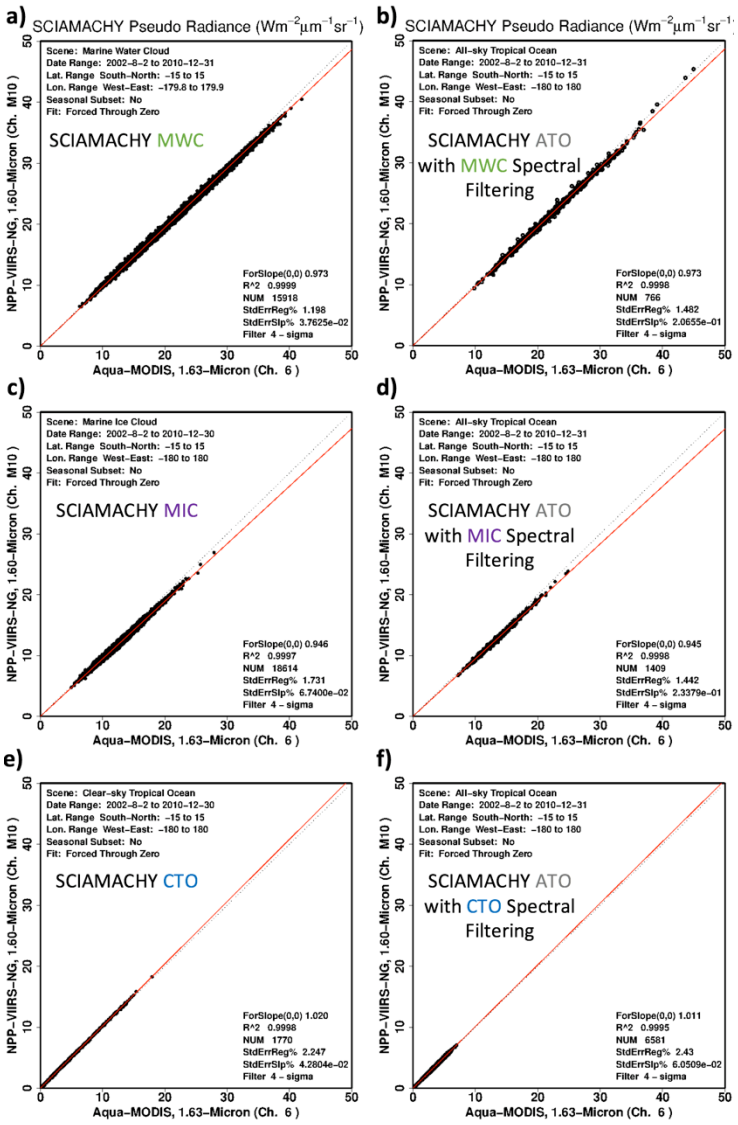

Figure 7. Same as Fig. 6, except instead for Aqua-MODIS band 6 and NPP-VIIRS band M10.

Figure 8 gives a more detailed look at the double spectral filtering capability and output of the spectra plotting tool. Here we see the same ATO with MIC spectral filtering scene as shown in Fig. 5d. Below the plot, the tool displays two tables. The top table within Fig. 8 reveals both the pseudo radiance and pseudo reflectance values corresponding to each of one's chosen SRF convolutions. A ratio of either the two SRF pseudo radiance or pseudo reflectance values is comparable to an SBAF based on the ratio of the mean energy from all SCIAMACHY footprints of that scene criteria. Although such an SBAF has its applications, it has no consideration for higher-order dependencies. That is, SBAFs between certain channels are often dependent on the magnitude of scene reflectance or radiance. For this reason, when an accurate SBAF is required, we recommend using the dedicated SBAF computation tool, which allows for higher-order adjustments. The Fig. 8 bottom table also provides radiance and reflectance values, but rather than pseudo instrument values based on SRFs, these results are based on the mean energy within the chosen spectral filter ranges. In other words, one can imagine radiance/reflectance convolution over an SRF of magnitude 1.0 for all wavelength values within the indicated spectral filter range (SF_range). Being able to parse any selected Earth-reflected spectra and compute pseudo/mean radiance/reflectance values in these ways can prove useful for determining energy thresholds when selecting scene type filters for bands in which scene composition cannot be easily distinguished by the radiance or reflectance value.

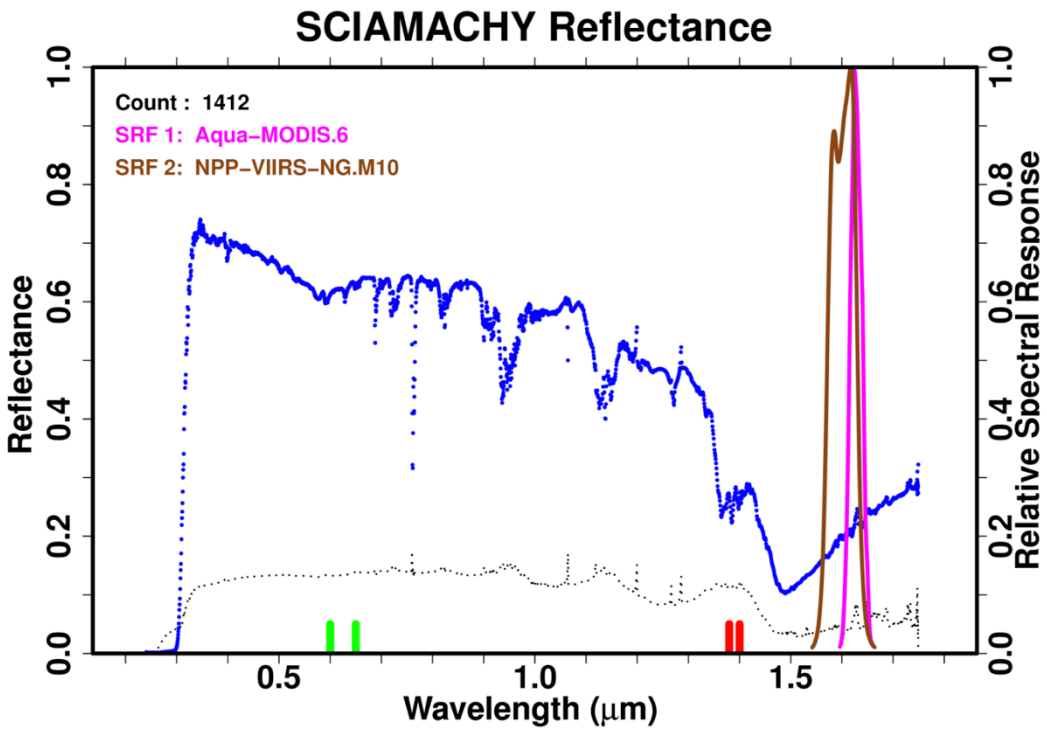

All-sky Tropical Ocean

	Name	Pseudo_Radiance	Pseudo_Reflectance
SRF 1	Aqua-MODIS.6	13.278	0.2201
SRF 2	NPP-VIIRS-NG.M10	12.539	0.1971

Note: Pseudo_Radiance Units: Watts per (meter^2-steradian-micron)

	SF_Range	SF_Radiance	SF_Reflectance
Spectral Filter 1	1.38 - 1.4	24.141	0.2554
Spectral Filter 2	0.6 - 0.65	278.280	0.6213

Note: SF_Radiance Units: Watts per (meter^2-steradian-micron)
Note: SF_Range Units: micron

Figure 8. Example SCIAMACHY spectral plotting tool output using the ATO Earth-reflected spectra with MIC-specific spectral filtering (same as Fig. 5d). The pink and brown rows in the first table provide pseudo radiance and reflectance values corresponding to the chosen SRFs. Similarly, the red and green rows of the second table provide mean radiance and reflectance values corresponding to the chose spectral filter ranges (x-axis colored tick-mark bounds).

3. RESULTS AND DISCUSSION

The annual regressions of the Aqua-MODIS/NPP-VIIRS SNO scaling ratios for ATO, MWC, MIC, and CTO scenes for 0.65-μm (MODIS band 1, VIIRS band M5) and 1.6-μm (MODIS band 6, VIIRS band M10) channel pairs, before application of an SBAF, are shown in Fig. 9. The MWC, MIC, and CTO SNO pairs are each a subset of the ATO comparison, based on the same filtering criteria used to separate the MWC, MIC, and CTO target SBAFs from the ATO scene SBAF as detailed in Table 1. Without an SBAF, spectral dependency on scene type in the comparison region dominates, and thus there is no common calibration ratio amongst the scene conditions for either channel. For example, in the 0.65-μm comparison, although the ATO and MIC mean scaling ratios are nearly the same, both are distinct from either the MWC or CTO scene scaling ratios with a difference of 0.015-0.021. The maximum scaling ratio difference, which is seen between MWC and CTO, is 0.036. Similarly, for the 1.6-μm comparison, the nearest mean scaling ratio comparison is between ATO and MWC scenes with a difference of 0.012. Relative to MIC, ATO differs by 0.024 and MWC differs by 0.036. The maximum difference, observed between MIC and CTO, is 0.092. From these results it is evident that spectral absorption disparity caused by scene dependency alone can account for 1.5% and 3.9% standard deviation uncertainty in the MODIS/VIIRS calibration gain for the 0.65-μm and 1.6-μm channels, respectively (e.g., standard deviation of 1.0033, 0.9885, 1.0035, and 1.0247 from Figs. 9a-9d).

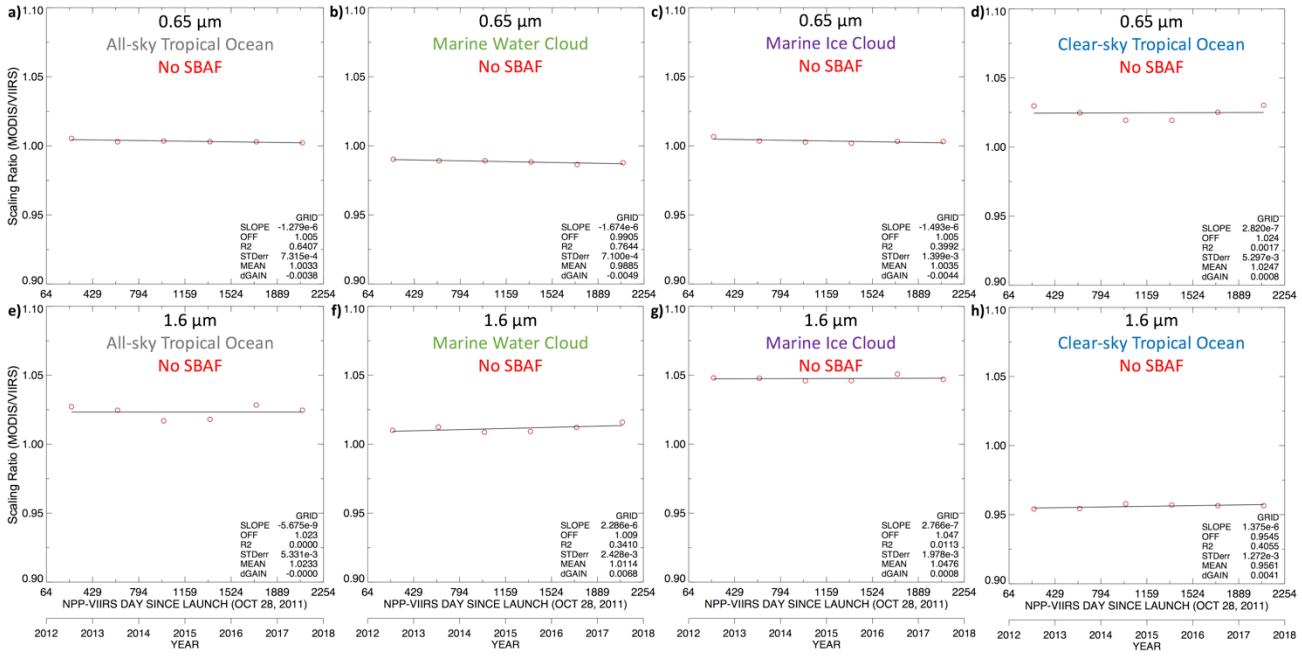

Figure 9. Yearly regression of the Aqua-MODIS and NPP-VIIRS SNO scaling ratio (MODIS/VIIRS) relationship for ATO, MWC, MIC, and CTO scenes for 0.65-µm (top) and 1.6-µm (bottom) channel pairs, without SBAF application.

Figure 10 shows the same annual regressions of the Aqua-MODIS/NPP-VIIRS SNO scaling ratios after application of an appropriate SBAF. The MWC and MIC scenes use the linear SBAF that is forced through the origin (i.e., force slope SBAF), which is the same as the ratio of the mean pseudo radiance for each sensor, as shown in Figs. 6b and 6d for the 0.65-µm channel, and Figs. 7b and 7d for the 1.6-µm channel. The force slope SBAF was also initially applied for the ATO and CTO scenes (Figs. 4b and 6e for 0.65-µm, Figs. 4c and 7e for 1.6-µm), and although they offered improvement, a 2nd-order nonlinear SBAF for ATO and a 1st-order "free" linear (slope and offset) SBAF for CTO are likely more effective choices. The reason they are better choices is because, unlike for MWC and MIC, the ATO scene radiance relationship between MODIS and VIIRS is highly a function of its magnitude, with a significantly different degree of correction required for dark scenes as opposed to bright scenes. The 2nd-order SBAF better captures both the bright and dark ends of the dynamic range (Fig. 11b) than the force slope SBAF (Fig. 11a). Similarly, for the CTO scenes, the force slope SBAF does not accurately depict the offset correlation of the MODIS/VIIRS SNO pairs for these darker radiances, and misses both the darkest and brightest ends of the matched pair comparisons (Fig. 11c). The 1st-order free linear SBAF, however, better represents the full dynamic range of points (Fig. 11d). Substitution with the higher-order fits is also supported by the change in the regression standard error (STDErrReg%) shown in the lower right corner of the Fig. 11 plots. For the ATO scene, the regression standard error reduction from the force slope SBAF to the 2nd-order fit SBAF is from 1.21% (Fig. 11a) to 0.94% (Fig. 11b), and for the CTO scene, the reduction is from 1.86% (Fig. 11c) to 1.00% (Fig. 11d). The regression standard error quantifies the uncertainty of the SBAF, revealing whether the inter-calibration conditions are accurately selected from the SBAF tool. A reduction in uncertainty suggests that the SBAF characterization for the scene has improved.

After the appropriate SBAFs were applied, the 0.65-µm channel mean scaling ratio difference between MWC and MIC reduced from 0.015 to 0.001, which is new the maximum difference observed among all four of the scene conditions. The ATO scaling ratio is now positioned between that for MWC and MIC, which is expected if the 2nd-order SBAF is accurately representing both scenes types in the ATO case, and if the individual MWC and MIC SBAFs are accurate. Also, the CTO scaling ratio fell by 0.04 to now align with the other three scenes. Ultimately for the 0.65-µm channel, the spectral filtering allows for accurate discrimination of the MWC, MIC, and CTO targets from the ATO scene, which when combined with the SBAFs derived from the same form of spectral filtering reduced the MODIS/VIIRS calibration gain standard deviation uncertainty from 1.5% to 0.5%.

For the 1.6-µm channel, the MWC and MIC mean scaling ratios reduced by 0.027 and 0.058, respectively, lowering their relative difference from 0.036 before to 0.006 after SBAF is applied. The ATO scaling ratio fell by 0.033, but is

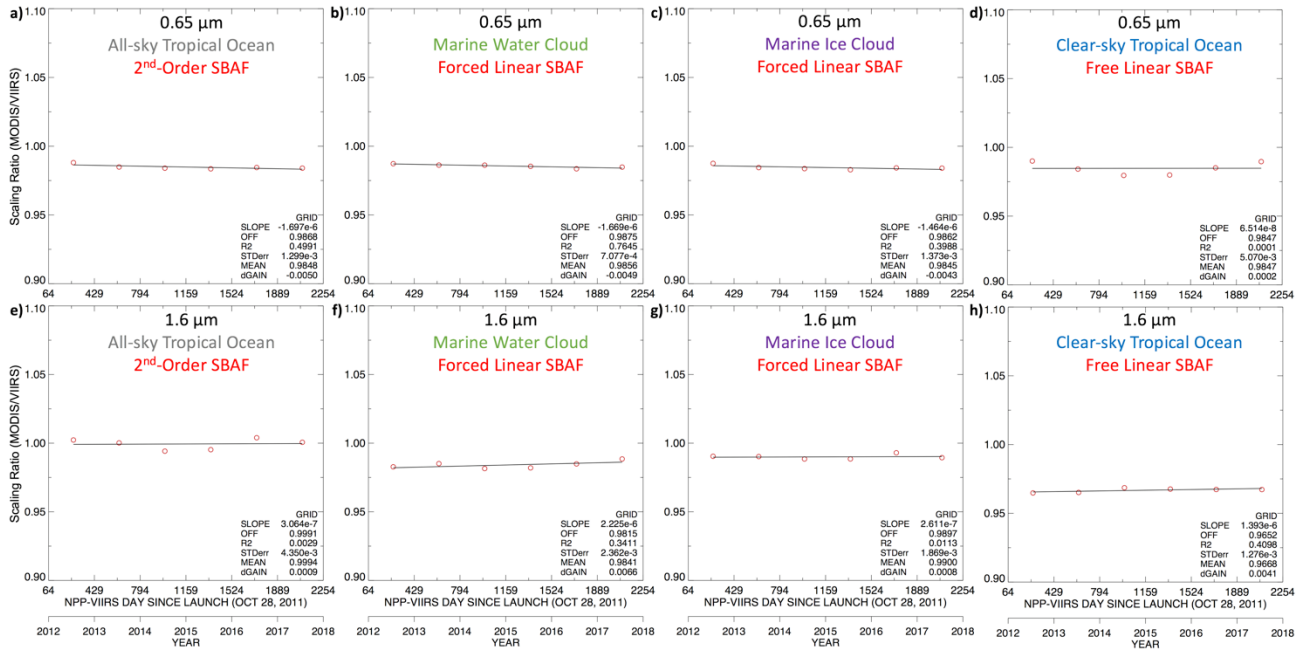

Figure 10. Same as Fig. 9, except with a 2nd-order non-linear SBAF applied for the ATO scenes, a linear SBAF forced through the origin applied for the the MWC and MIC scenes, and a 1st-order "free" linear (slope and offset) SBAF applied for the CTO scenes.

still 0.015 or 0.009 higher than that for MWC or MIC, respectively. This result is not unexpected given that for 1.6-µm wavelengths, the different scenes are not as neatly stratified as a function of radiance as they are for 0.65-µm channels, and it is this exact problem that the spectral filtering tools are designed to mitigate. Because MWC and MIC are not easily separated from ATO based on radiance alone, there is no reasonable expectation that a 2nd-order SBAF applied to the ATO scene should account for the spectral disparity of both individual scenes. Separating each scene using spectral filtering, and applying the specific SBAFs, yields mean ratios that are more aligned with one-another than when trying to account for the spectral disparity of the all-inclusive ATO target. The CTO scaling ratio, however, does not align with those of MWC and MIC. Although the SBAF adjusted the CTO mean ratio toward the right direction, the magnitude of correction is insufficient. Relative to without SBAF application, the calibration gain standard deviation uncertainty when considering MWC, MIC, and CTO reduced from 4.6% to 1.2% (3.9% to 1.4% when also considering ATO). Although the reduction is effective, CTO is still an outlier compared to MWC and MIC, which align rather well. The reason for the disparate CTO scaling ratio results may be due to the fact that dark CTO targets are simply too hard to detect in actual practice. That is, the response at the sensors for such low radiance values is difficult to accurately quantify given the detector sensitivity at these wavelengths. In application, however, this result is of little consequence as we can faithfully rely on the gains derived from the brighter targets, i.e., the clouds.

4. CONCLUSIONS

A database-driven, open-access online tool (*https://satcorps.larc.nasa.gov/SBAF*) satisfies a critical need of the GSICS organization and the broader calibration community by allowing users freedom to design SBAFs unique to their calibration requirements, with many options for precise control. This improved SBAF tool, when combined with the enhanced features of the SCIAMACHY spectra plotting tool, found at *https://satcorps.larc.nasa.gov* under the *Langley Satellite Calibration* link, allows for robust, energy-based scene-type selection for bands that may not be sensitive to well-defined measurement thresholds, and for which determining the proper SBAF is a challenge. That is, for certain instrument channels (e.g., those near 1.6-µm), separating scene conditions is not as easily accomplished by simple radiance/reflectance stratification as it is for other bands (e.g., those near 0.65-µm and 1.38-µm). By using those more scene-energy-dependent bands, however, and limiting their consideration based on certain radiance/reflectance thresholds, we are able to separate scene conditions in the less energy-stratified channels via proxy, and apply a target-specific SBAF. Consistency of Aqua-MODIS/NPP-VIIRS spectrally filtered SNO calibration coefficients achieved via

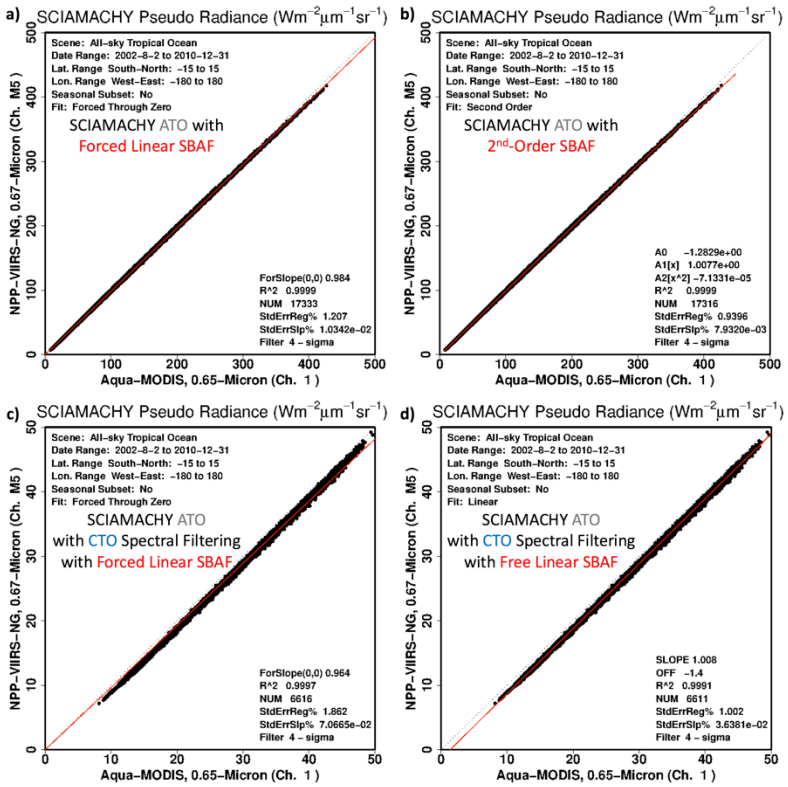

Figure 11. a) The 0.65-μm channel pseudo radiance pair force slope SBAF regression for the ATO scene (same as Fig. 4b). b) same as a) except instead showing the 2nd-order nonlinear SBAF. c) The 0.65-μm channel pseudo radiance pair force slope SBAF regression for the CTO scene (magnified version of Fig. 6f). d) same as c) except instead showing the 1st-order "free" linear (slope and offset) SBAF. Both b) and c) better capture the full dynamic range of the regression as opposed to the force slope SBAF variants.

careful SBAF selection based on the same spectral filtering for varied scene types serves as a simple validation of the approach, and as an application demonstration of the enhanced SBAF tool features.

Users can visualize the available SCIAMACHY mean hyperspectral radiance or reflectance Earth-reflected spectra signature with the spectra plotting tool. Furthermore, users have the ability to change specific aspects of the plotted spectra in order to make it more relevant to their calibration scenario. Of particular benefit is the spectral filtering capability, which allows specification of what footprint spectra are included in the mean signature by removing spectra with energy values beyond stated thresholds within a defined wavelength range. With two of these spectral filters, scene conditions can be more accurately distinguished for a chosen channel based on energy level stratification at separate wavelengths. Using this technique then with the spectral filtering capability of the SBAF tool allows production of scene-specific SBAFs that can be applied to actual, spectrally filtered data.

We used the Aqua-MODIS/NPP-VIIRS SNO scaling ratios to test the scene separation capability of the spectral filters and assess the SBAF performance. The spectral filter thresholds determined from the spectra plotting tool were used with actual MODIS/VIIRS 0.65-μm and 1.6-μm channel SNO data over ATO scenes in order to separate the MWC, MIC, and CTO targets. We then applied 0.65-μm and 1.6-μm channel SBAFs based on the same spectral filter thresholds in order to see if the same mean scaling ratio is predicted for the separated scenes. For the 0.65-μm channel, the scene separation and SBAF application worked rather well, reducing an initial maximum difference in average scaling ratio between ATO, MWC, MIC, and CTO from 0.036 before SBAF application to within 0.001 after SBAF application, with a standard deviation uncertainty reduction from 1.5% to 0.5%. Results are less uniform for the 1.6-μm channel, although the technique was still effective. The mean scaling difference for MWC and MIC scenes fell from 0.036 before to 0.006 after SBAF was applied, which are 0.009-0.015 less than the same for ATO after SBAF application. This result, however, is not unexpected given that for 1.6-μm wavelengths, the separated targets are not neatly stratified as a function of energy, so there is not a reasonable expectation that an SBAF applied to the ATO scene should fully account for the

spectral discrepancy. One may have expected better agreement between either MWC or MIC with CTO scaling ratios, between the three of which exists a 1.2% standard deviation uncertainty (down from 4.6% before SBAF application), but this discrepancy might be owed to the idea that the dark 1.6-μm CTO targets are simply too difficult to detect in practice. Fortunately, there are the brighter cloud targets to rely upon, which do agree well within this technique for these wavelengths. Ultimately, these enhanced spectral filtering features of the spectra plotting and SBAF calculation tools, along with the other tool options, offer unprecedented simplicity and flexibility in producing precise spectral corrections, and should prove to be of great value to the calibration community.

ACKNOWLEDGMENTS

This work was supported by the NASA Research Opportunities in Space and Earth Sciences for Satellite Calibration Interconsistency Studies and the NASA Clouds and the Earth's Radiant Energy System (CERES) project.

REFERENCES

[1] Scarino, B. R., D. R. Doelling, P. Minnis, A. Gopalan, T. Chee, R. Bhatt, C. Lukashin, and C. O. Haney, "A web-based tool for calculating spectral band difference adjustment factors derived from SCIAMACHY hyperspectral data," IEEE Trans. Geosci. Remote Sens., vol. 54, no. 5, pp. 2529-2542 (2016).

[2] Goldberg, M., G. Ohring, J. Butler, C. Cao, R. Datla, D. Doelling, V. Gärtner, T. Hewison, B. Iacovazzi, D. Kim, T. Kurino, J. Lafeuille, P. Minnis, D. Renaut, J. Schmetz, D. Tobin, L. Wang, F. Weng, X. Wu, F. Yu, P. Zhang, and T. Zhu, "The Global Space-based Inter-Calibration System (GSICS)," Bull. Amer. Meteor. Soc. 92(4), 467-475 (2011).

[3] Chander, G., N. Mishra, D. L. Helder, D. B. Aaron, A. Angal, T. Choi, X. Xiong, and D. Doelling, "Applications and limitations of Spectral Band Adjustment Factors (SBAF) for cross-calibration," IEEE Trans. Geosci. Remote Sens., 53(3), 1267-1281, (2013).

[4] Slater, P. N., S. F. Biggar, R. G. Holm, R. D. Jackson, Y. Moa, M. S. Moran, J. M. Palmer, and B. Yuan, "Reflectance- and radiance-based methods for the in-flight absolute calibration of multispectral sensors," Remote Sens. Environ., 22(11), 11-37, (1987).

[5] Slater, P. N., S. F. Biggar, K. J. Thome, D. I. Gellman, and P. R. Spyak, "Vicarious radiometric calibrations of EOS sensors," J. Atmos. Oceanic Technol., 13, 349-359, (1996).

[6] Teillet, P. M., G. Fedosejevs, R. P Gauthier, N. T. O'Niel, K. J. Thome, S. F. Biggar, H. Ripley, and A. Meygret, "A generalized approach to the vicarious calibration of multiple Earth observation sensors using hyperspectral data," Remote Sens. Environ., 77, 304-327, (2001).

[7] Henry, P., G. Chander, B. Fougnie, C. Thomas, and X. Xiong, "Assessment of spectral band impact on intercalibration over desert sites using simulation based on EO-1 Hyperion data," IEEE Trans. Geosci. Remote Sens, 51(3), (2013).

[8] Czapla-Myers, J., J. McCorkel, N. Anderson, K. Thome, S. Biggar, D. Helder, D. Aaron, L. Leigh, and N. Mishra, "The ground-based absolute radiometric calibration of Landsat 8 OLI," Remote Sens., 7, (2015).

[9] Doelling, D. R., C. Lukashin, P. Minnis, B. Scarino, and D. Morstad, "Spectral reflectance corrections for satellite intercalibrations using SCIAMACHY data," Geosci. Remote Sens. Lett., 8, (2011).

[10] Scarino, B.R., D. R. Doelling, D. L. Morstad, R. Bhatt, A. Gopalan, C. Luakshin, and P. Minnis, "Using SCIAMACHY to improve corrections for spectral band differences when transferring calibration between visible sensors," Proc. SPIE, 8510, (2012).

[11] Doelling, D. R., "Vis/NIR inter-calibration product announcements," GSICS Users Workshop, https://gsics.nesdis.noaa.gov/wiki/Development/UsersWorkshop2015, (2015).

[12] Wielicki, B. A. and co-authors, "Achieving climate change absolute accuracy in orbit," Bull. Amer. Meteor. Soc., 94(10), 1519-1539, (2013).

[13] Doelling, D.R., C.O. Haney, B.R. Scarino, A. Gopalan, and R. Bhatt, "Improvements to the geostationary visible imager ray-matching calibration algorithm for CERES edition 4," J. Atmos. Oceanic Technol., Vol. 33 No. 12, pp. 2679-2698, DOI: 10.1175/JTECH-D-16-0113.1, (2016).

[14] Global Space-based Inter-Calibration System: GRWG VIS/NIR Web Meeting 2018-07-05, "GSICS Web Meeting on VIIRS as a Reference," http://gsics.atmos.umd.edu/bin/view/Development/20180705 (2018).